

Mutant *GNAS* limits tumor aggressiveness in established
pancreatic cancer via antagonizing the KRAS-pathway
(GNAS 変異は KRAS 経路に拮抗することにより、
膵癌の悪性度を抑える)


旭川医科大学大学院医学系研究科博士課程
医学専攻

河端 秀賢

(Yusuke Ono, Nobue Tamamura, Kyohei Oyama, Jun Ueda, Hiroki Sato, Kenji Takahashi,
Kenzui Taniue, Tetsuhiro Okada, Syugo Fujibayashi, Akihiro Hayashi, Takuma Goto,
Katsuro Enomoto, Hiroaki Konishi, Mikihiro Fujiya, Keita Miyakawa, Mishie Tanino,
Yuji Nishikawa, Daisuke Koga, Tsuyoshi Watanabe, Chiho Maeda, Hidenori Karasaki,
Andrew S. Liss, Yusuke Mizukami, Toshikatsu Okumura)



Mutant *GNAS* limits tumor aggressiveness in established pancreatic cancer via antagonizing the *KRAS*-pathway

Hidemasa Kawabata¹ · Yusuke Ono^{1,7} · Nobue Tamamura¹ · Kyohei Oyama² · Jun Ueda³ · Hiroki Sato^{1,9} · Kenji Takahashi¹ · Kenzui Taniue^{1,8} · Tetsuhiro Okada¹ · Syugo Fujibayashi¹ · Akihiro Hayashi¹ · Takuma Goto¹ · Katsuro Enomoto¹ · Hiroaki Konishi¹ · Mikihiro Fujiya¹ · Keita Miyakawa⁴ · Mishie Tanino⁴ · Yuji Nishikawa⁵ · Daisuke Koga⁶ · Tsuyoshi Watanabe⁶ · Chiho Maeda⁷ · Hidenori Karasaki⁷ · Andrew S. Liss⁹ · Yusuke Mizukami^{1,7}  · Toshikatsu Okumura¹

Received: 14 October 2021 / Accepted: 25 December 2021
© Japanese Society of Gastroenterology 2022

Abstract

Background Mutations in *GNAS* drive pancreatic tumorigenesis and frequently occur in intraductal papillary mucinous neoplasm (IPMN); however, their value as a therapeutic target is yet to be determined. This study aimed at evaluating the involvement of mutant *GNAS* in tumor aggressiveness in established pancreatic cancer.

Methods CRISPR/Cas9-mediated *GNAS* R201H silencing was performed using human primary IPMN-associated pancreatic cancer cells. The role of oncogenic *GNAS* in tumor maintenance was evaluated by conducting cell

culture and xenograft experiments, and western blotting and transcriptome analyses were performed to uncover *GNAS*-driven signatures.

Results Xenografts of *GNAS* wild-type cells were characterized by a higher Ki-67 labeling index relative to *GNAS*-mutant cells. Phenotypic alterations in the *GNAS* wild-type tumors resulted in a significant reduction in mucin production accompanied by solid with massive stromal components. Transcriptional profiling suggested an apparent conflict of mutant *GNAS* with *KRAS* signaling. A significantly higher Notch intercellular domain (NICD) was observed in the nuclear fraction of *GNAS* wild-type cells. Meanwhile, inhibition of protein kinase A (PKA) induced NICD in *GNAS*-mutant IPMN cells, suggesting that NOTCH signaling is negatively regulated by the *GNAS*-PKA pathway. *GNAS* wild-type cells were characterized by a significant invasive property relative to *GNAS*-mutant cells, which was mediated through the NOTCH regulatory pathway.

Conclusions Oncogenic *GNAS* induces mucin production, not only via MUC2 but also via MUC5AC/B, which may enlarge cystic lesions in the pancreas. The mutation may also limit tumor aggressiveness by attenuating NOTCH signaling; therefore, such tumor-suppressing effects must be considered when therapeutically inhibiting the *GNAS* pathway.

Keywords Intraductal papillary mucinous neoplasm · Primary culture · *GNAS* · NOTCH

✉ Yusuke Mizukami
mizu@asahikawa-med.ac.jp

¹ Department of Medicine, Asahikawa Medical University, 2-1 Midorigaoka Higashi, Asahikawa, Hokkaido 078-8510, Japan

² Department of Cardiovascular Surgery, Asahikawa Medical University, Asahikawa, Hokkaido 078-8510, Japan

³ Department of Advanced Medical Science, Asahikawa Medical University, Asahikawa, Hokkaido 078-8510, Japan

⁴ Department of Surgical Pathology, Asahikawa Medical University, Asahikawa, Hokkaido 078-8510, Japan

⁵ Division of Tumor Pathology, Department of Pathology, Asahikawa Medical University, Asahikawa, Hokkaido 078-8510, Japan

⁶ Department of Microscopic Anatomy and Cell Biology, Asahikawa Medical University, Asahikawa, Hokkaido 078-8510, Japan

⁷ Institute of Biomedical Research, Sapporo-Higashi Tokushukai Hospital, Sapporo, Hokkaido 065-0033, Japan

⁸ Isotope Science Center, The University of Tokyo, Tokyo 113-0032, Japan

⁹ Division of Gastrointestinal and Oncologic Surgery, Massachusetts General Hospital, Boston, MA 02114, USA

Introduction

Pancreatic ductal adenocarcinoma, one of the most lethal cancers in the world [1, 2], is associated with two main types of morphologically distinct precursors: pancreatic intraepithelial neoplasia (PanIN) and intraductal papillary mucinous neoplasm (IPMN) [3, 4]. *KRAS* is a ubiquitous genetic alteration leading to these precursors, whereas mutations in *GNAS* are unique to IPMN [5, 6]. The *GNAS* gene encodes the stimulatory G-protein alpha-subunit G(s) α of heterotrimeric G-protein-coupled receptor signaling. Ligand stimulation induces adenylyl cyclase, generating the second messenger cAMP, which is a protein kinase A (PKA) activator. In many tissues, GNAS–cAMP signaling maintains quiescence and cellular differentiation [7–9], and approximately 41–75% of human IPMN exhibits recurrent gain-of-function mutations in the pathway [10, 11]. Histologically, oncogenic *GNAS* is closely related to intraluminal mucin production and papillary growth and is more significantly associated with intestinal-type IPMN, which is characterized by MUC2 expression, relative to other epithelial types [12].

GNAS is mutationally activated in multiple tumor types, such as villous adenoma of the colorectum [13], a subgroup of inflammatory liver tumors [14], and mucinous and non-mucinous lung adenocarcinomas [15], and the oncogenic mechanisms can be diverse. Genetically engineered mouse models in the context of mutant *KRAS* suggested crosstalk among driver mutations during pancreatic tumorigenesis, and induction of mutant *GNAS* alone in mouse pancreas could initiate tumorigenesis, and the process can be significantly accelerated in the presence of mutant *KRAS* [16–18]. GNAS–PKA signaling also exhibits a tissue-specific tumor suppressor function by blocking the GLI and YAP oncogenic transcriptional regulators [19, 20]. In addition, in colorectal tumorigenesis, the oncogenic role of *GNAS* is crucial in certain phases of tumor development and may no longer be required once the biological advantage gained by the other genetic and epigenetic alterations compensates for tumor maintenance [21]. Therefore, it is essential to determine the downstream program during *GNAS*-mediated tumorigenesis and understand this dichotomy between “oncogenic” and “tumor-suppressive” functions in established tumors.

Despite the accumulating evidence on the oncogenic role of *GNAS* brought by integrated pathological analysis in combination with mutation profiling using resected specimens [22–24], the details of the molecular mechanisms associated with the emergence of IPMN and tumor progression in humans have not been fully elucidated owing to the scarcity of human IPMN-derived cell lines [18, 25]. Such knowledge is vital to characterizing the

tumor biology related to the GNAS pathway and developing novel diagnostic tests that may capitalize on these data. Here, we aim to understand the role of oncogenic *GNAS* mutations in tumor maintenance. Utilizing human cells from IPMN and Cas9-mediated genome editing of mutant *GNAS* allele into wild type will allow us to assess the detailed signaling pathways interacting with the canonical *KRAS*-driven signaling.

Methods

Human IPMN cells and tissue

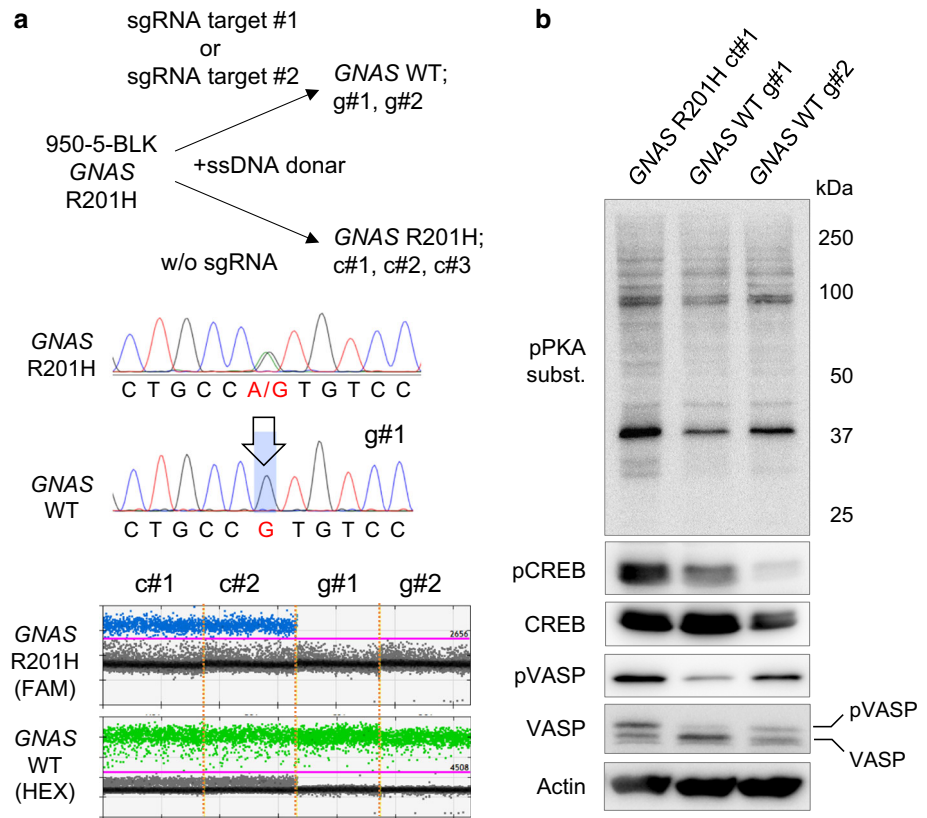
We utilized 950-5-BLK cells harboring heterozygous *KRAS* G12V and *GNAS* R201H mutations [18]. For monolayer culture, cells were grown in Gibco DMEM/F-12 (Dulbecco’s modified Eagle’s medium/Ham’s F-12 Nutrient Mixture, #11330057, Thermo Fisher Scientific, Waltham, MA, USA) supplemented with 10% fetal bovine serum (Biosera, Nuaille, France) and 100 U/mL penicillin–streptomycin (Cat: 168-23191, FUJIFILM Wako Chemicals, Japan) at 37 °C with 5% CO₂ and passaged at 70–80% confluence. For three-dimensional (3D)-organoid growth assays, we utilized Matrigel overlay methods with the following supplements: 2% bovine serum albumin (#034-25462, FUJIFILM Wako Chemicals), 1 × Insulin–Transferrin–Selenium (ITS-G; #090-06741, FUJIFILM Wako Chemicals), 10 μ M ROCK inhibitor Y-27632 (#030-24021, FUJIFILM Wako Chemicals), and diluted 2% Matrigel (#354262, Corning, Tewksbury, MA, USA). Protein isolation and immunoblotting was carried out according to previously reported protocols (Supplementary Methods).

Patient specimens from surgically resected pancreatic cancer samples were used based on a protocol approved by the Institutional Review Board (IRB) of Asahikawa Medical University (#17002). Written informed consent was obtained from all patients prior to enrollment.

Generation of GNAS R201H CRISPR knockout cells

Two distinct sets of oligonucleotides encoding gRNAs against human *GNAS* 201H (guide#1 and guide#2) were cloned into pSpCas9(BB)-2A-Puro (PX459) V2.0 (Addgene #62988; Table S1 shows sequences) [26]. Single-strand donor DNA [ssDNA; Integrated DNA Technologies (IDT)] was utilized to restore the wild-type allele genomic sequence with a 60 bp 3′- and 5′-homologous arm (Fig. S1). The outline of the CRISPR/Cas9-mediated specific knockout targeting the *GNAS* R201H allele is illustrated in Fig. 1a and Supplementary Methods.

Fig. 1 Mutant *GNAS*-specific silencing in human IPMN cells. **a** Approach to CRISPR/Cas9-mediated genome editing targeting *GNAS* R201H. Two different single-guide RNAs (sgRNAs) were utilized (more details in Fig. S1). **b** Immunoblot showing PKA regulation in IPMN cells as determined by phosphorylation of CREB and VASP, VASP mobility shift (PKA-phosphorylated VASP), and using an anti-phospho-PKA substrate (Subst.)



shRNA-mediated knockdown of MUC2 and MUC5B

Knockdown was performed using pLKO-based lentiviral shRNA vectors designed by the RNAi Consortium (BROAD Institute), and purchased from Merck KGaA (Darmstadt, Germany). pLKO.1-GFP was used as a control (Addgene, #30323). Lentiviruses were produced in 293T cells using standard protocols with packaging plasmids (pxPAX2 and pMD2.G) as described previously [18]. The shRNA targeting sequences are shown in Table S1.

Growth assay and xenograft

We assessed tumor cell phenotypes via monolayer and organoid cultures, as well as with scratch and invasion assays (Supplementary Methods). For subcutaneous xenograft studies, 8-week-old female severe combined immune deficient (SCID) mice (CB17/Icr-*Prkdc*^{scid}/CrI/Crlj; Charles River Laboratories, Yokohama, Japan) were used.

Gene expression profiling

For RNA-sequencing (RNA-seq) studies, total RNA was isolated in duplicate from two independent lines grown in the 3D-culture using the RNeasy mini kit (QIAGEN, Hilden, Germany). RNA-seq library preparation and

sequencing were performed using the Ion GeneStudio S5 system (Thermo Fisher Scientific). Gene set enrichment analysis (GSEA) was used to analyze the enrichment of functional gene groups [27]. Quantitative reverse transcription-PCR was performed to validate the expression. A detailed procedure for these experiments is described in the Supplementary Methods.

Statistical analysis and image processing

In all cases, results are expressed as mean \pm standard deviation. Statistical significance was determined using a two-tailed Student's *t*-test, where a *P* value < 0.05 was considered statistically significant. All statistical calculations were performed using R (version 3.3.2; The R Foundation for Statistical Computing) and Prism9 (GraphPad Software). The proliferation index was evaluated using Ki-67 immunohistochemical staining images, and positive cells were counted using Fiji ImageJ based on color deconvolution [28].

Results

Mutant *GNAS*-specific silencing

To study the tumor maintenance role of oncogenic *GNAS*, we generated paired human IPMN cells harboring mutant and wild-type (WT) *GNAS*. Due to the lack of pancreatic cancer cells with mutant *GNAS* in globally used cell banks, 950-5-BLK, an in-house cellular resource from pancreatic cancer patient-derived xenografts (PDXs), was used [18].

For Cas9-mediated genome editing, two different guide RNAs were utilized, and two *GNAS*-WT cells from 950-5-BLK cells were established (Fig. 1a, Fig. S1, Table S1). In addition to Sanger sequencing, a digital PCR assay was performed to validate the complete silencing of the R201H allele.

Next, we performed immunoblot analyses to examine whether specific knockdown of mutant *GNAS* abrogates the canonical cAMP-PKA-driven pathway. Lysates from *GNAS*-WT IPMN cells exhibited significant downregulation of phosphorylated-substrates of PKA relative to the *GNAS*-mutant cells (Fig. 1b). Furthermore, phosphorylation of vasodilator-stimulated phosphoprotein and cAMP-responsive element-binding protein, which are downstream effectors of PKA, was also inhibited by silencing mutant *GNAS*, suggesting that the mutation plays an important role in regulating canonical PKA signaling (Fig. 1b).

Effect of silencing of mutant *GNAS* on IPMN cell growth in vitro

We determined whether mutant *GNAS* provides a growth advantage in human IPMN cells. An in vitro growth assay was performed on a monolayer with a complete medium or 3D-organoid culture in serum-free conditions (Fig. 2a). In contrast to *GNAS*-mutant cells with a tight margin of the cell cluster, the cell-cell attachment of *GNAS*-WT cells appeared to be weak. The monolayer culture of Cas9-mediated *GNAS* R201H knockout IPMN cells was not impaired relative to the control *GNAS*-mutant 950 cells; instead, both *GNAS*-WT subclones grew better than the control cells (Fig. 2b). Furthermore, 3D-culture *GNAS*-mutant 950 cells in Matrigel were represented by substantial bubbles appearing as a cystic component (Fig. 2a). The majority of *GNAS*-WT organoids were characterized by solid lumps and grew more rapidly on day 4 (Fig. 2b).

Mutant *GNAS* inducing mucin production and suppressing in vivo growth of IPMN cells

We conducted xenograft experiments to observe the in vivo phenotypes of human IPMN cells. Similar to the organoid

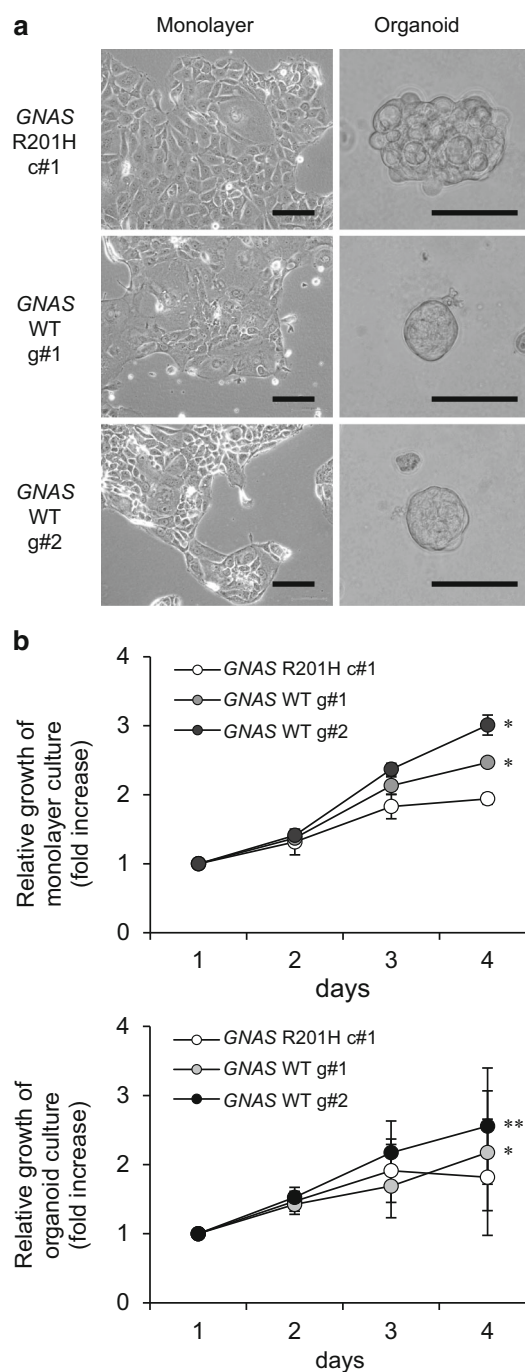


Fig. 2 Effect of silencing of mutant *GNAS* on in vitro growth of IPMN cells. **a** Monolayer and organoid cultures established from two independent *GNAS*-WT cells (g#1 and g#2) were tested. Scale: 100 μ m. **b** Relative growth of IPMN cells harboring mutant- and WT-*GNAS*. Shown is the mean \pm SD. *P* value of a two-tailed unpaired *t*-test **P* < 0.05. *P* value, ***P* < 0.01

culture, *GNAS*-mutant 950 cells established xenografts with multiple cystic components (Fig. 3a). Scanning electron microscopy of the tumors showed differences in the characteristics of the mucinous lumen as hollows, suggesting abundant mucin production. In contrast, *GNAS*-WT

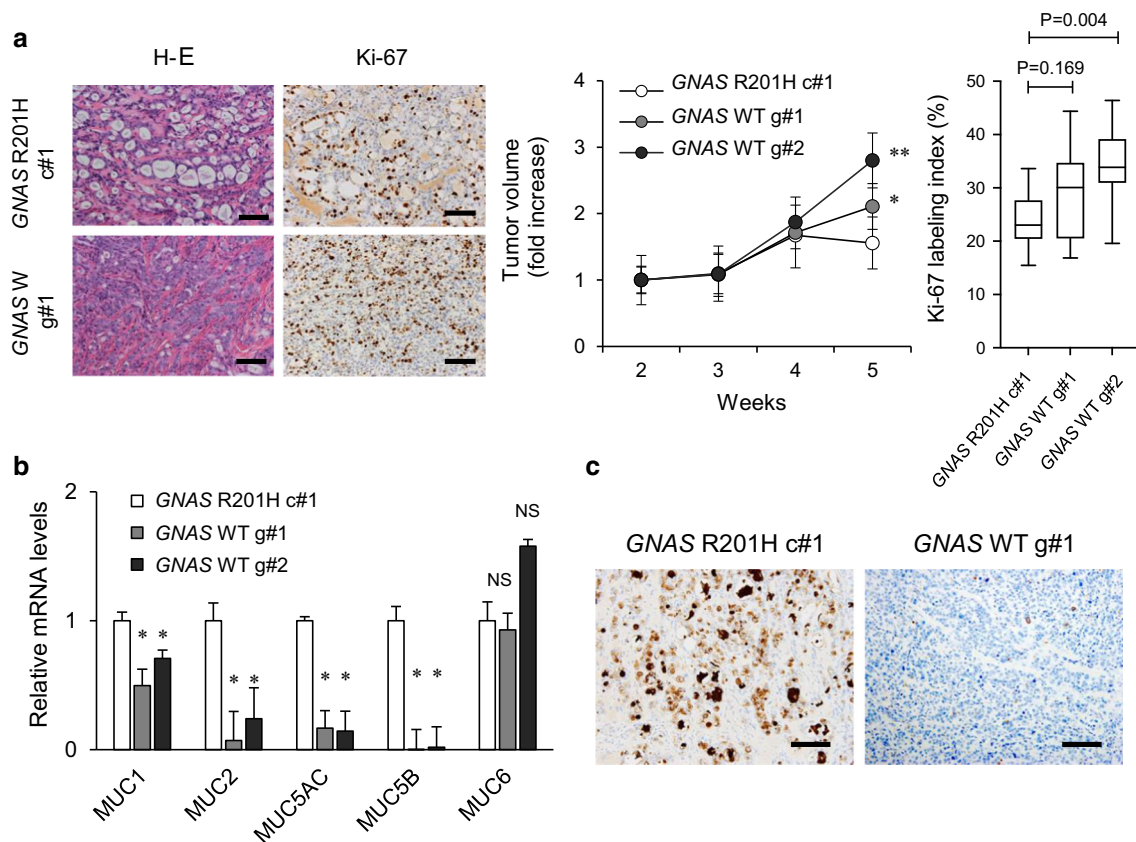
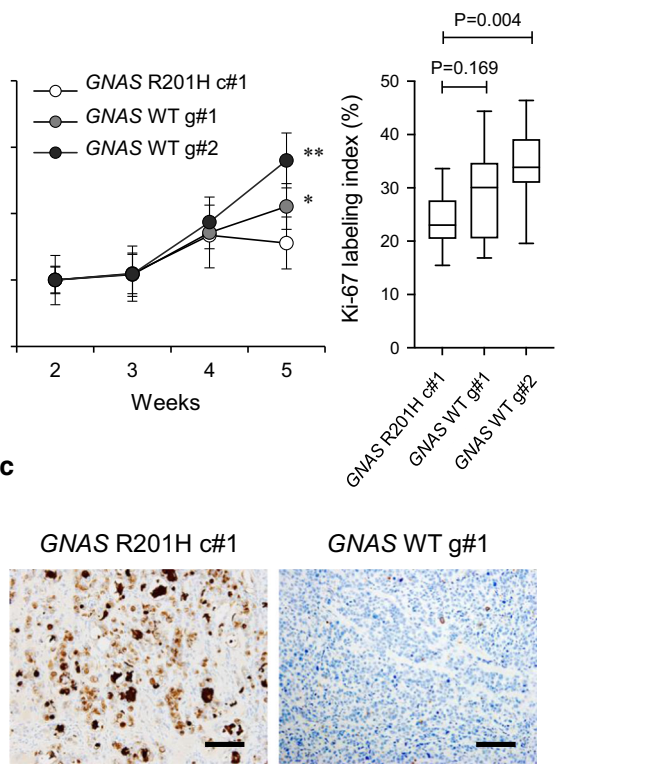


Fig. 3 Mutant *GNAS* inducing mucin production and suppressing in vivo growth of IPMN cells. **a** Xenograft tumors from *GNAS*-mutant (c#1) and *GNAS*-WT (g#1) isolated 5 weeks after implantation were analyzed by H&E staining and immunostaining using anti-Ki-67. Scale: 100 μ m. Weekly measurement of xenograft volume was normalized 2 weeks after the implantation. *N* = 4 mice per group. *P* value of a two-tailed unpaired *t*-test vs. *GNAS* R201H xenograft



P* = 0.268, *P* = 0.016. Ki-67 labeling index was quantified using the ImageJ software. **b** qRT-PCR analysis showing relative expression of MUC1, 2, 5AC, 5B, and 6 in IPMN cells engineered with Cas9 and the indicated sgRNAs. *P* value of a two-tailed unpaired *t*-test **P* < 0.01. NS; not significant. **c** Immunostaining using anti-MUC5B in *GNAS*-mutant and -WT xenografts of IPMN cells. Scale: 100 μ m

950 cells formed dense solid tumors with massive stromal components.

The tumor growth rate of *GNAS*-WT xenografts was higher than that of *GNAS*-mutant tumors (*P* = 0.268, WT#g1; *P* = 0.016, WT#g2; Fig. 3a). Immunohistochemistry for Ki-67 was performed to evaluate the proliferation of tumor cells in the xenografts. Consistent with the larger tumor size and more solid components, *GNAS*-WT xenografts were marked by a higher Ki-67-labeling index, albeit less significant in *GNAS*-WT#g1 tumors.

Given the hyper-mucin-producing phenotype in *GNAS*-mutant tumors, quantitative analyses of genes associated with mucin synthesis were performed using *GNAS*-mutant and *GNAS*-WT 950 cells. In addition to MUC2, qPCR assay demonstrated a significant expression of MUC5AC and MUC5B mRNA in *GNAS*-mutant cells relative to the *GNAS*-WT cells. In contrast, the difference between MUC1 and MUC6 was modest (Fig. 3b). Immunostaining of patients' IPMN specimens and PDXs with mutant *GNAS* also demonstrated strong MUC5AC/MUC5B expression

despite MUC2 staining (Fig. S4). A larger dataset from the Cancer Genome Atlas utilizing *GNAS*-mutant and *GNAS*-WT pancreatic cancer tissue specimens also indicated striking differences in the expression of MUC2 and MUC5B mRNAs but not in that of MUC1 (Fig. S3).

Mutant *GNAS*-oriented transcriptome opposing *KRAS* signatures

Considering the significance of co-existing driver mutations *KRAS* and *GNAS* in human IPMN cells, we speculated about the crosstalk among oncogenes. GSEA was performed using the RNA-seq dataset from the *GNAS*-mutant (c#1, c#2, c#3) and the *GNAS*-WT cells (g#1, g#2) (Fig. 4a). Using hallmark gene sets [29], several significantly enriched sets were identified in both *GNAS*-edited IPMN cells harboring the WT allele relative to the *GNAS*-mutant cells (Table 1). Among the robustly upregulated gene set in *GNAS*-WT cells, we were interested in “Hallmark *KRAS* SIGNALING UP” because it suggests the

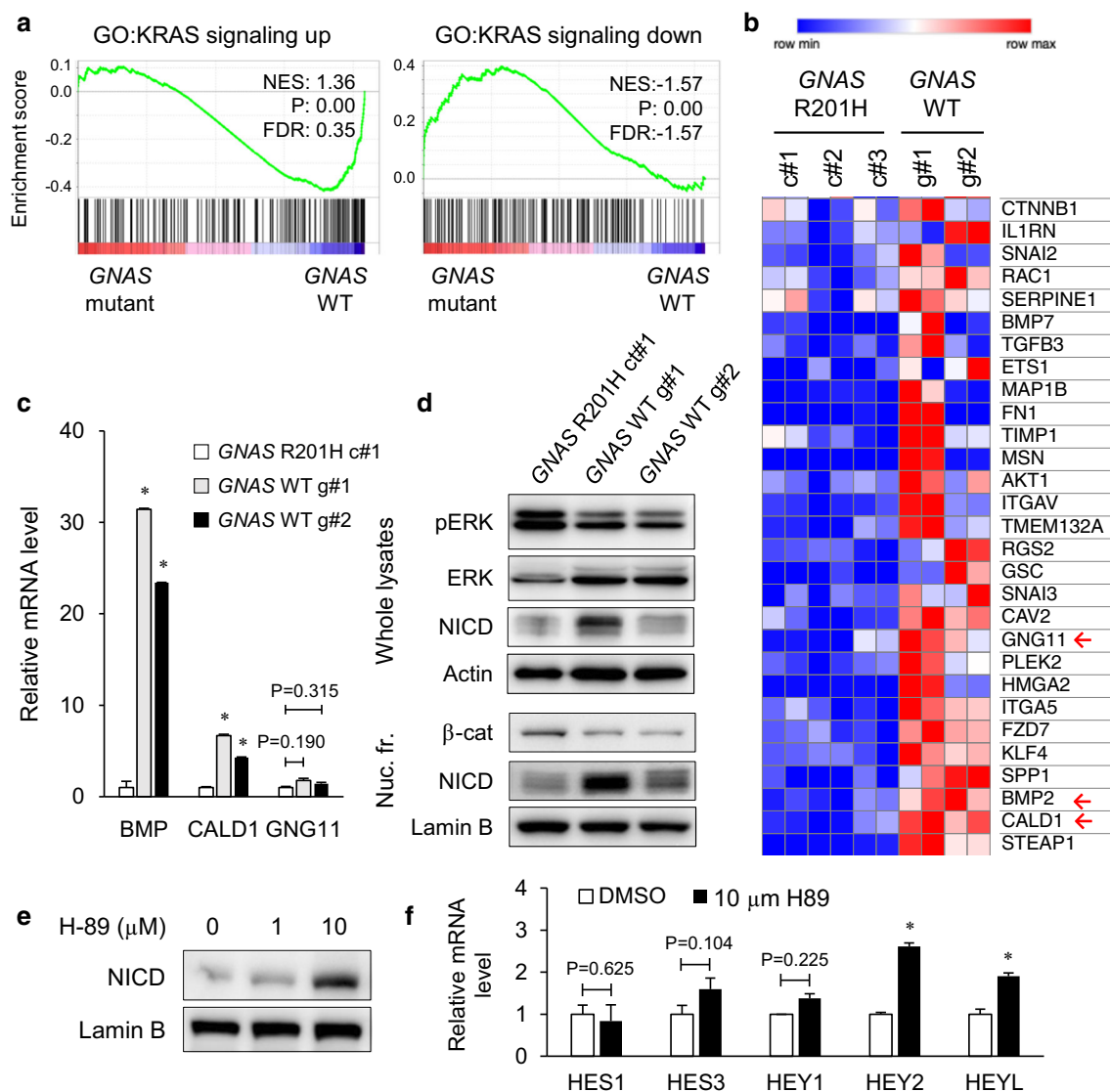


Fig. 4 Mutant *GNAS*-oriented transcriptome opposing *KRAS* signatures and blocking NOTCH pathway. **a** GSEA was performed using RNA-seq data from *GNAS*-WT (g#1 and g#2) and *GNAS*-mutant organoid lines (c#1, #2 and #3) grown in Matrigel. *GNAS* R201H negatively regulates *KRAS* signaling categories from the Gene Ontology (GO) database. **b** Abundance of EMT-related genes detected by RNA-seq data in *GNAS*-WT organoid lines relative to the *GNAS*-mutant lines. mRNA levels are shown as log₂ ratio of intensity over the average intensity across all samples of the studied

cell line in each experiment. Heatmap of 29 genes assigned as core enrichment is shown. **c** RNA isolated from the indicated IPMN lines was examined by qRT-PCR analysis for the indicated genes. **P* < 0.01 vs. c#1. **d** Immunoblot using whole lysates and nuclear fraction (fr.) from IPMN cells as determined by ERK phosphorylation, Notch intracellular domain (NICD) expression, and nuclear accumulation of β-catenin. **e, f** Effect of PKA inhibition by H-89 on nuclear localization of NICD (**e**) and induction levels of the HES/HEY genes (**f**). **P* < 0.05 vs. DMSO

antagonistic effects of oncogenic *GNAS* against *KRAS* signaling (Fig. 4a). However, the only gene set enriched in *GNAS*-mutant IPMN cells was “Hallmark *KRAS* SIGNALING DOWN,” although the value of FDR was over 25% (Fig. 4a, Table 2; *P* = 0.000).

Another gene set specifically enriched in *GNAS*-WT cells relative to the mutant counterpart was of genes related to the Myc targets, PI3K/AKT/mTOR signaling, and G2/M checkpoint, supporting their growth advantage (Table 1a). Besides these gene sets associated with cell proliferation,

genes related to the epithelial–mesenchymal transition (EMT) were more closely associated with IPMN cells harboring WT-*GNAS* in comparison to the mutant cells (FDR = 17%), although the difference was not statistically significant (*P* = 0.225). We then utilized another gene set associated with EMT to evaluate whether the silencing of mutant *GNAS* affects this signature more precisely (Fig. 4b, Table S4). The qPCR analysis demonstrated the robust upregulation of BMP2 and CALD1 mRNA by silencing mutant *GNAS*. These results indicate that mutant

Table 1 Top 30 gene sets enriched in GNAS-WT IPMN cells

	GS follow link to MSigDB	Size	ES	NES	NOM p-val	FDR q-val	FWER p-val	Rank at max	Leading edge
1	HALLMARK_E2F_TARGETS	193	- 0.75	- 1.77	0	0.02	0.012	2150	tags = 55%, list = 10%, signal = 61%
2	HALLMARK_INTERFERON_GAMMA_RESPONSE	195	- 0.6	- 1.77	0	0.014	0.019	3438	tags = 49%, list = 17%, signal = 58%
3	HALLMARK_INTERFERON_ALPHA_RESPONSE	93	- 0.66	- 1.77	0	0.011	0.019	2937	tags = 56%, list = 14%, signal = 65%
4	HALLMARK_ALLOGRAFT_REJECTION	193	- 0.46	- 1.75	0	0.01	0.019	3482	tags = 30%, list = 17%, signal = 35%
5	HALLMARK_MYC_TARGETS_V1	194	- 0.7	- 1.67	0	0.019	0.037	4227	tags = 70%, list = 20%, signal = 87%
6	HALLMARK_G2M_CHECKPOINT	189	- 0.64	- 1.65	0	0.022	0.062	1718	tags = 44%, list = 8%, signal = 47%
7	HALLMARK_MYC_TARGETS_V2	58	- 0.64	- 1.64	0.006	0.02	0.062	2478	tags = 53%, list = 12%, signal = 61%
8	HALLMARK_COMPLEMENT	195	- 0.46	- 1.61	0	0.024	0.08	2891	tags = 29%, list = 14%, signal = 34%
9	HALLMARK_KRAS_SIGNALING_UP	192	- 0.42	- 1.57	0	0.037	0.124	2945	tags = 29%, list = 14%, signal = 33%
10	HALLMARK_IL6_JAK_STAT3_SIGNALING	86	- 0.52	- 1.56	0.018	0.039	0.124	3158	tags = 34%, list = 15%, signal = 40%
11	HALLMARK_MTORC1_SIGNALING	193	- 0.58	- 1.53	0	0.048	0.163	3993	tags = 51%, list = 19%, signal = 63%
12	HALLMARK_INFLAMMATORY_RESPONSE	192	- 0.48	- 1.51	0	0.051	0.18	3240	tags = 33%, list = 16%, signal = 39%
13	HALLMARK_ANDROGEN_RESPONSE	95	- 0.45	- 1.48	0.013	0.063	0.218	3019	tags = 35%, list = 15%, signal = 40%
14	HALLMARK_IL2_STAT5_SIGNALING	192	- 0.41	- 1.45	0	0.085	0.287	3715	tags = 33%, list = 18%, signal = 40%
15	HALLMARK_FATTY_ACID_METABOLISM	155	- 0.47	- 1.44	0.006	0.084	0.304	3988	tags = 44%, list = 19%, signal = 54%
16	HALLMARK_PI3K_AKT_MTOR_SIGNALING	104	- 0.37	- 1.41	0	0.105	0.358	4039	tags = 33%, list = 19%, signal = 40%
17	HALLMARK_GLYCOLYSIS	193	- 0.41	- 1.39	0.028	0.119	0.416	3926	tags = 37%, list = 19%, signal = 46%
18	HALLMARK_APOPTOSIS	158	- 0.44	- 1.39	0.029	0.115	0.422	4515	tags = 43%, list = 22%, signal = 55%
19	HALLMARK_DNA_REPAIR	141	- 0.38	- 1.37	0.052	0.128	0.458	2862	tags = 28%, list = 14%, signal = 32%

Table 1 continued

GS follow link to MSigDB	Size	ES	NES	NOM p-val	FDR q-val	FWER p-val	Rank at max	Leading edge
20 HALLMARK_WNT_BETA_CATENIN_SIGNALING	42	- 0.41	- 1.37	0.074	0.123	0.463	3779	tags = 36%, list = 18%, signal = 44%
21 HALLMARK_OXIDATIVE_PHOSPHORYLATION	182	- 0.56	- 1.34	0.144	0.142	0.497	4533	tags = 58%, list = 22%, signal = 74%
22 HALLMARK_UV_RESPONSE_UP	151	- 0.39	- 1.33	0.032	0.152	0.521	4626	tags = 44%, list = 22%, signal = 57%
23 HALLMARK_SPERMATOGENESIS	131	- 0.37	- 1.32	0.089	0.149	0.539	2897	tags = 19%, list = 14%, signal = 22%
24 HALLMARK_REACTIVE_OXYGEN_SPECIES_PATHWAY	47	- 0.49	- 1.29	0.214	0.168	0.596	4728	tags = 55%, list = 23%, signal = 71%
25 HALLMARK_EPITHELIAL_MESENCHYMAL_TRANSITION	194	- 0.4	- 1.28	0.225	0.17	0.613	3840	tags = 37%, list = 18%, signal = 44%
26 HALLMARK_COAGULATION	137	- 0.36	- 1.27	0.193	0.181	0.643	3145	tags = 29%, list = 15%, signal = 34%
27 HALLMARK_PEROXISOME	103	- 0.37	- 1.27	0.12	0.175	0.643	4921	tags = 38%, list = 24%, signal = 49%
28 HALLMARK_ESTROGEN_RESPONSE_LATE	190	- 0.35	- 1.26	0.054	0.174	0.643	3630	tags = 34%, list = 17%, signal = 40%
29 HALLMARK_XENOBIOTIC_METABOLISM	197	- 0.34	- 1.25	0	0.179	0.675	4260	tags = 30%, list = 20%, signal = 37%
30 HALLMARK_APICAL_SURFACE	43	- 0.37	- 1.25	0.041	0.176	0.675	2791	tags = 26%, list = 13%, signal = 29%

Table 2 Gene sets enriched in *GNAS*-mutant IPMN cells

	GS follow link to MSigDB	Size	ES	NES	NOM p-val	FDR q-val	FWER p-val	Rank at max	Leading edge
1	HALLMARK_KRAS_SIGNALING_DN	187	0.4	1.36	0	0.352	0.584	5826	tags = 32%, list = 28%, signal = 44%
2	HALLMARK_MYOGENESIS	196	0.25	1.03	0.354	1	0.993	2447	tags = 16%, list = 12%, signal = 18%
3	HALLMARK_PROTEIN_SECRETION	95	0.28	0.97	0.479	1	1	5009	tags = 38%, list = 24%, signal = 50%
4	HALLMARK_UV_RESPONSE_DN	138	0.29	0.94	0.565	0.956	1	5483	tags = 36%, list = 26%, signal = 48%
5	HALLMARK_TGF_BETA_SIGNALING	54	0.28	0.91	0.597	0.845	1	3796	tags = 28%, list = 18%, signal = 34%
6	HALLMARK_NOTCH_SIGNALING	32	0.27	0.9	0.755	0.722	1	3798	tags = 28%, list = 18%, signal = 34%
7	HALLMARK_UNFOLDED_PROTEIN_RESPONSE	107	0.27	0.82	0.722	0.746	1	4097	tags = 35%, list = 20%, signal = 43%

GNAS may partially limit tumor aggressiveness despite the established tumor-initiating roles (Fig. 4c).

Synergistic and antagonistic effect of mutant *GNAS* on the *KRAS* path

Given the significant oncogenic effects of *GNAS* R201C/H in the context of mutant *KRAS* [16, 18], we evaluated the crosstalk using protein immunoblot analyses. Significant phosphorylation of extracellular-signal-regulated kinase (ERK) and nuclear accumulation of β -catenin were observed in *GNAS*-mutant cells relative to *GNAS*-WT cells, suggesting synergistic crosstalk between mutant *KRAS* and *GNAS* (Fig. 4d).

Since canonical NOTCH signaling is required for tumor initiation and progression in *KRAS*-driven pancreatic carcinogenesis [30, 31], we next analyzed the intracellular domain of the Notch intercellular domain (NICD) (Fig. 4d). The expression was modest in mutant *GNAS* cells, and strong NICD expression was observed in the *GNAS*-WT cells. Immunoblot analysis using nuclear protein demonstrated significantly higher expression in *GNAS*-WT cells than in the *GNAS*-mutant counterpart (Fig. 4d), and the nuclear expression in *GNAS*-WT cells was comparable to that in pancreatic cancer cell lines harboring WT *GNAS* and mutant *KRAS* (Fig. S5). To evaluate whether the suppression of NICD expression was mediated through the

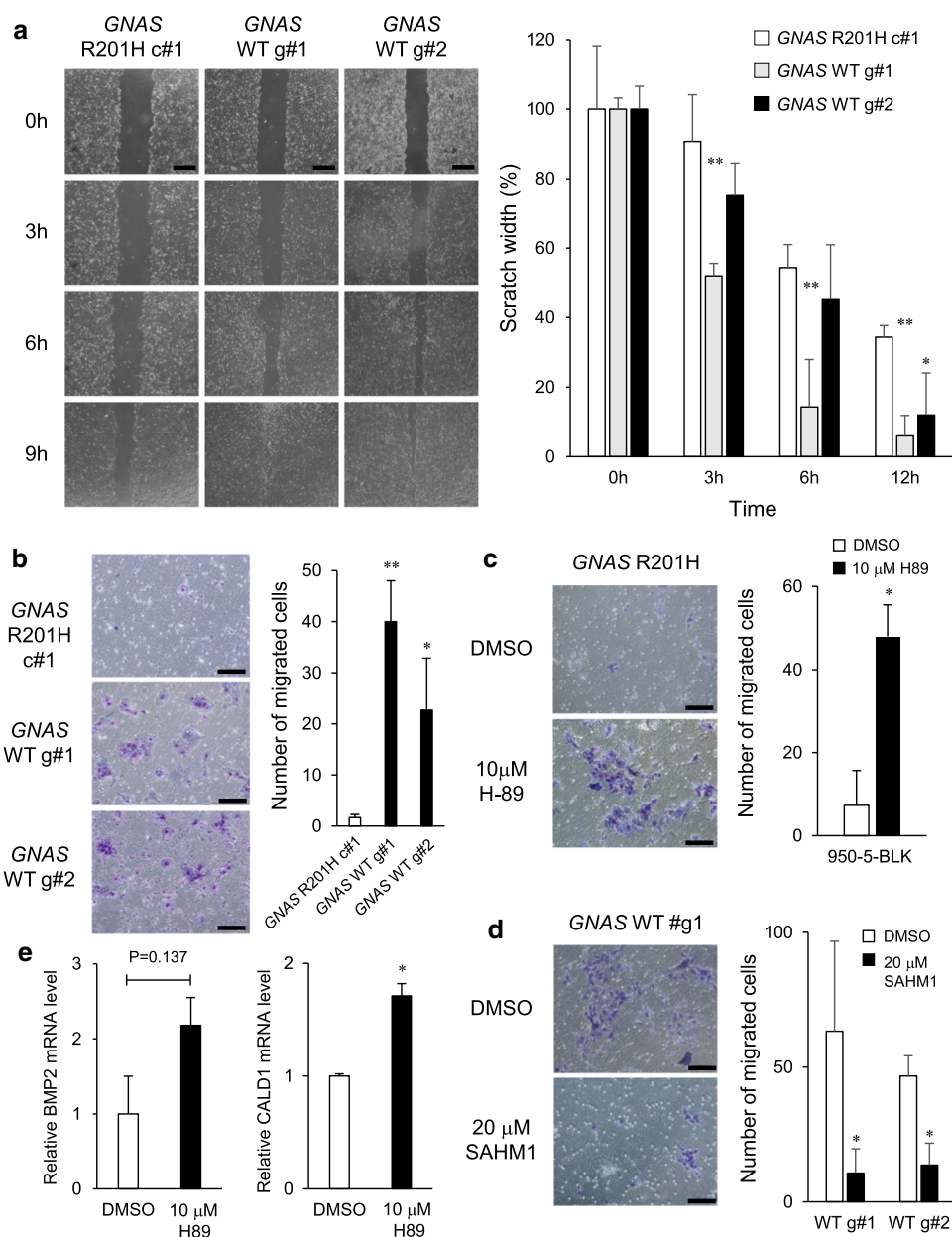
GNAS-PKA axis, the effect of PKA inhibition was tested. Pretreatment of *GNAS*-mutant IPMN cells with 10 μ M H-89 markedly induced NICD (Fig. 4e) and subsets of NOTCH targeted HEY family transcripts, HEY1, HEY2, and HEYL (Fig. 4f), suggesting that NOTCH inhibition by oncogenic *GNAS* was PKA-dependent.

To dissect the molecular pathway regulating MUC2 and MUC5B, the effect of inhibition of these *KRAS* paths was tested. SCH772984, a potent and selective ERK inhibitor, suppressed the expression of MUC2 but not of MUC5B. In contrast, inhibition of PKA significantly restrained the expression of not only MUC2 but also of MUC5B, suggesting that MUC5B may be induced independently of the PKA-ERK axis. In addition, inhibition of NOTCH in *GNAS*-WT IPMN cells induced MUC5B (Fig. S6).

Oncogenic *GNAS* suppresses tumor invasiveness through attenuating NOTCH signaling

Finally, we evaluated whether oncogenic *GNAS* may actively attenuate *KRAS*-driven aggressive tumor properties. Scratch wound healing and transwell invasion assays were performed because some of the EMT-related genes were downregulated in *GNAS*-mutant IPMN cells relative to the *GNAS*-WT cells (Fig. 5a). There was a reduction in the scratch size after 6 h in *GNAS*-WT cells, and the wound was completely closed at 24 h, whereas the wound closure

Fig. 5 Mutant *GNAS* suppresses invasiveness via NOTCH signaling. **a, b** Scratch wound healing (**a**) and Transwell invasion assay (**b**) were performed. Scale: 500 μm (**a**), 100 μm (**b**). * $P < 0.05$, ** $P < 0.01$ vs. c#1. **c, d** Effect of an inhibitor of PKA, H-89 (**c**), and of NOTCH transcription factor complex, SAHM1 (**d**), on *GNAS*-mutant and *GNAS*-WT cells was evaluated via invasion assay. * $P < 0.05$. **(e)** Effect of H-89 on BMP2 and CALD1 expression was evaluated via qRT-PCR. * $P < 0.05$



was incomplete in *GNAS*-mutant cells. Invasion through Matrigel demonstrated the aggressive invasive behavior of the *GNAS*-WT cells. In contrast, the invasive ability of *GNAS*-mutant IPMN cells was much lower and over 80% suppressed relative to the *GNAS*-WT counterparts (Fig. 5b).

We next evaluated the role of MUC2 and MUC5B in invasiveness. Organoids and xenografts from *GNAS*-mutant IPMN cells, infected with shMUC5B lentivirus, were characterized and exhibited significantly less mucin production, whereas the shMUC2 and shGFP tumors harbored abundant levels of mucin (Fig. S2a, b). Meanwhile, no significant difference was noted in the xenograft size. Moreover, silencing of MUC2 and MUC5B in *GNAS*-

mutant IPMN cells did not significantly inhibit cell invasion (Fig. S2c).

Given the significant expression of NICD in *GNAS*-WT cells relative to that in the *GNAS*-mutant cells, we used SAHM1, which is a synthetic peptide that inhibits the NOTCH transcription factor complex, to examine whether the robust invasive property of *GNAS*-WT cells is mediated through NICD (Fig. 5d). SAHM1 suppressed the invasiveness of *GNAS*-edited cells and downregulated the expression of EMT-related genes (BMP2 and CALD1) in *GNAS*-mutant cells (Fig. 5e). Therefore, PKA-mediated blockade of the NOTCH pathway appeared to control tumor cell invasiveness as well as mucin production.

Discussion

Activating mutations of *GNAS* promote cell proliferation and early tumorigenesis; however, the mechanism by which this oncogene behaves to confer aggressive tumor phenotypes remains unclear. In the current study, we uncovered the novel tumor “braking” role of mutant *GNAS* by antagonizing the KRAS-pathway in part by suppressing NOTCH signaling. This finding is consistent with previous studies; *GNAS* can mediate a tissue-specific tumor suppressor function by inactivating the GLI and YAP oncogenic transcriptional regulators in a PKA-dependent manner [19, 20]. Moreover, exogenous expression of mutant *GNAS* suppresses cell growth in some human pancreatic cancer cells [32]. Therefore, this oncogene can inhibit a part of the cancer hallmarks, leading to limited aggressiveness.

The paradoxical effects of PKA signaling in tumors, acting as either a tumor suppressor or a promoter in different tumor types [33], may depend on the context of invasive/metastatic progression. Previous reports have suggested that PKA can lead to “mesenchymal-to-epithelial” transition and loss of tumor-initiating ability [34]. This effect was mediated through PHF2-dependent epigenetic reprogramming of tumor cells, resulting in their differentiation. Another potential target of PKA, resulting in the inhibition of tumor aggressiveness, is GLI2; phosphorylation by PKA can induce GLI2 processing and degradation [35]. Further epigenetic and proteomic studies are required to uncover the tumor-suppressing functions governed by oncogenic *GNAS*.

We demonstrated that oncogenic *GNAS* negatively regulates NOTCH signaling in a PKA-dependent manner; however, the precise mechanism underlying the inhibitory pathway remains to be determined. AMPK appears to be inhibited by PKA, which associates with and phosphorylates AMPK α 1 at Ser-173 to impede threonine (Thr-172) phosphorylation, resulting in the inactivation of AMPK α 1 during lipolytic signals [36]. NOTCH and its interaction with ubiquitin ligases have often been shown to be influenced by regulators, such as NUMB, which suppresses NOTCH signaling by recruiting Itchy E3 ubiquitin-protein ligase (ITCH) and facilitating the degradation of NICD [37]. Under hypoxic conditions, AMPK impairs the interaction between NICD and ITCH via tyrosine kinase Fyn, thus stabilizing the cleaved NOTCH by reducing its ubiquitination and degradation in breast cancer cells [38]. Therefore, the PKA-AMPK axis may facilitate NOTCH degradation through NUMB/ITCH. Furthermore, NUMB is an essential regulator of acinar cell differentiation and viability during acinar-to-ductal metaplasia, which results in PanIN in the context of oncogenic *KRAS* in mice [39].

However, more in-depth analysis is required to fully determine the role of PKA in NOTCH in human pancreatic tumors and how the crosstalk between *KRAS* and *GNAS* may affect the fate of tumor progression.

MUC5AC facilitates migration and invasion by regulating the function of E-cadherin in pancreatic cancer cells [40]. MUC5B can also promote cell proliferation and invasion of breast cancer cells when overexpressed [41]. In contrast, upregulation of another gel-forming mucin, MUC6, in early lesions associated with pancreatic cancer can inhibit the invasion of PanIN lesions through the basement membrane of the pancreatic duct, which slows the development of infiltrating carcinoma, whereas MUC6 expression is lost later in tumor progression [42]. However, in the current study, knockdown of MUC2 or MUC5B did not significantly affect the invasive property of tumor cells (Fig. S2c). We did not perform a double knockdown of these gel-forming mucins simultaneously. Nonetheless, a significant reduction in mucin production in the IPMN organoid and xenograft was observed upon MUC5B knockdown. Given the much higher copy number of MUC5B relative to that of MUC2 (Fig. S3), MUC5B might be more crucial to the enlargement of the cyst size during IPMN progression although previous literature demonstrates that MUC2 plays a critical role in inducing the histological character associated with the intestinal-type IPMN [12]. A recent study demonstrated that analysis of MUC5AC expression in circulating extracellular vesicles is practical for discriminating high-grade-IPMN from invasive carcinoma associated with IPMN to low-grade-IPMN and healthy subjects [43]. MUC5B may also be a useful marker if it can be feasibly detected in serum and pancreatic juice.

Our study has several limitations. First, we performed CRISPR/Cas9-mediated gene editing using a single line of human IPMN-derived cells harboring a heterozygous mutation in *GNAS* R201H. In addition, we used organoid culture and conditional reprogramming methods combined with PDXs to generate a panel of primary cell lines derived from surgical specimens of different grades of IPMN and associated pancreatic ductal adenocarcinoma [18, 44]. However, a limited number of lines harboring mutant *GNAS* could be established, and many of them could not be well tolerated during the genome editing process. Thus, in addition to providing essential insights into IPMN biology, upgrading human cell resources will provide a platform for further studies to define the molecular features predicting whether IPMNs have indolent versus aggressive potential. Second, although RNA-seq data suggest the antagonistic effect of mutant *GNAS* on the *KRAS* path, we identified the only NOTCH that can be affected differently between the two oncogenes. Oncogenic *GNAS* can also accelerate tumor-promoting pathways, such as MAPK and WNT

signaling [45, 46]; thus, complex crosstalk may independently exhibit tumor phenotypes. More detailed analyses using a larger number of patient's cellular resources from distinct stages of a tumor will be required to fully understand the interactions.

Oncogenic *GNAS* and its linked signaling circuitry may represent therapeutic cancer prevention and treatment targets [47]. However, GTPases remain undruggable because of the difficulty of displacing high-affinity guanine nucleotides and the lack of other drug-binding sites. In addition to these challenges, the results of our study and previous reports showing the tumor inhibitory role of *GNAS*-PKA signaling cause concerns for unconditional targeting of *GNAS* as chemotherapy. Given the significant tumor-initiating role of oncogenic *GNAS*, specific inhibition of the *GNAS*-PKA axis can help prevent tumor initiation and progression [48]. However, similar interventions may enhance tumor invasion and ultimate metastatic dissemination in later stages. A previous study also demonstrated that agents that elevated cellular cAMP levels and activated PKA markedly diminished the migration and Matrigel invasion of human pancreatic cancer cells by inhibiting RhoA and RhoC activity [49]. Exchange protein directly activated by cAMP (EPAC) is another intracellular receptor that mediates the effects of second messenger cAMP induced by mutant *GNAS* [50], and EPAC1 has been represented as a potential target for novel therapeutic strategies to develop anti-metastasis agents for pancreatic cancer [51]. Therefore, selective inhibition of downstream molecules of mutant *GNAS*, which eliminates deleterious tumor-promoting, but not tumor-suppressing, effects, would be an ideal targeted therapy. Considering the development of several promising compounds targeting NOTCH intracellular domain [52], combinations with such inhibitors may be alternatively considered when PKA signaling needs to be directly targeted to suppress oncogenic *GNAS*.

In conclusion, oncogenic *GNAS* induces unique mucin-producing properties in pancreatic tumor cells but attenuates their invasiveness. The latter "tumor-suppressive" effect is mediated by blocking NOTCH signaling. Enlarged cyst size in IPMN of the pancreas due to abundant mucin production may not always indicate an aggressive tumor, but somewhat biologically limited aggressiveness.

Supplementary Information The online version contains supplementary material available at <https://doi.org/10.1007/s00535-021-01846-4>.

Acknowledgements We would like to thank Rika Kakisaka and Atsuko Nishikawa (Sapporo Higashi Tokushukai Hospital) for performing IHC quantification of the xenografts; Ayumu Sugitani (Sapporo Higashi Tokushukai Hospital) for supporting statistical analyses; and Eiko Aoyanagi (Sapporo Higashi Tokushukai Hospital) for tissue sample preparation. We also thank Krushna C. Patra

(Department of Cancer Biology at University of Cincinnati) for critical reading of the manuscript.

Funding This work was supported by Pancreas Research Foundation of Japan and Grants-in-Aid for Regional R&D Proposal-Based Program from Northern Advancement Center for Science & Technology of Hokkaido in Japan (to H. Kawabata) and by JSPS KAKENHI Grant Number 20K17009 (to H. Kawabata), 20K07671 (to Y.O.), 20K09070 (to H. Karasaki) and 20H03655 (to Y.M.).

Declarations

Conflict of interest YO and YM receive funding from Hitachi High-Tech Corporation. The other authors declare that they have no known competing financial interests or personal relationships that could have appeared to influence the work reported in this paper.

References

- Bray F, Ferlay J, Soerjomataram I, et al. Global cancer statistics 2018: GLOBOCAN estimates of incidence and mortality worldwide for 36 cancers in 185 countries. *CA Cancer J Clin*. 2018;68:394–424.
- Siegel RL, Miller KD, Jemal A. Cancer statistics, 2020. *CA Cancer J Clin*. 2020;70:7–30.
- Basturk O, Hong SM, Wood LD, et al. A revised classification system and recommendations from the Baltimore consensus meeting for neoplastic precursor lesions in the pancreas. *Am J Surg Pathol*. 2015;39:1730–41.
- Ren B, Liu X, Suriawinata AA. Pancreatic ductal adenocarcinoma and its precursor lesions: histopathology, cytopathology, and molecular pathology. *Am J Pathol*. 2019;189:9–21.
- Ryan DP, Hong TS, Bardeesy N. Pancreatic adenocarcinoma. *N Engl J Med*. 2014;371:1039–49.
- Patra KC, Bardeesy N, Mizukami Y. Diversity of precursor lesions for pancreatic cancer: the genetics and biology of intraductal papillary mucinous neoplasm. *Clin Transl Gastroenterol*. 2017;8:e86.
- Watanabe K, Nakamura T, Onodera S, et al. A novel *GNAS*-mutated human induced pluripotent stem cell model for understanding *GNAS*-mutated tumors. *Tumour Biol*. 2020;42:1010428320962588.
- Drelon C, Berthon A, Sahut-Barnola I, et al. PKA inhibits WNT signalling in adrenal cortex zonation and prevents malignant tumour development. *Nat Commun*. 2016;7:12751.
- Xing F, Luan Y, Cai J, et al. The anti-Warburg effect elicited by the cAMP-PGC1 α pathway drives differentiation of glioblastoma cells into astrocytes. *Cell Rep*. 2017;18:468–81.
- Furukawa T, Kuboki Y, Tanji E, et al. Whole-exome sequencing uncovers frequent *GNAS* mutations in intraductal papillary mucinous neoplasms of the pancreas. *Sci Rep*. 2011;1:161.
- Wu J, Matthaei H, Maitra A, et al. Recurrent *GNAS* mutations define an unexpected pathway for pancreatic cyst development. *Sci Transl Med*. 2011;3:92ra66.
- Omori Y, Ono Y, Kobayashi T, et al. How does intestinal-type intraductal papillary mucinous neoplasm emerge? *CDX2* plays a critical role in the process of intestinal differentiation and progression. *Virchows Arch*. 2020;477:21–31.
- Yamada M, Sekine S, Ogawa R, et al. Frequent activating *GNAS* mutations in villous adenoma of the colorectum. *J Pathol*. 2012;228:113–8.
- Nault JC, Fabre M, Couchy G, et al. *GNAS*-activating mutations define a rare subgroup of inflammatory liver tumors characterized by *STAT3* activation. *J Hepatol*. 2012;56:184–91.

15. Ritterhouse LL, Vivero M, Mino-Kenudson M, et al. GNAS mutations in primary mucinous and non-mucinous lung adenocarcinomas. *Mod Pathol*. 2017;30:1720–7.
16. Taki K, Ohmuraya M, Tanji E, et al. GNAS(R201H) and Kras(G12D) cooperate to promote murine pancreatic tumorigenesis recapitulating human intraductal papillary mucinous neoplasm. *Oncogene*. 2016;35:2407–12.
17. Ideno N, Yamaguchi H, Ghosh B, et al. GNAS(R201C) induces pancreatic cystic neoplasms in mice that express activated kras by inhibiting YAP1 signaling. *Gastroenterology*. 2018;155:1593–1607 e12.
18. Patra KC, Kato Y, Mizukami Y, et al. Mutant GNAS drives pancreatic tumorigenesis by inducing PKA-mediated SIK suppression and reprogramming lipid metabolism. *Nat Cell Biol*. 2018;20:811–22.
19. He X, Zhang L, Chen Y, et al. The G protein alpha subunit Galphas is a tumor suppressor in Sonic hedgehog-driven medulloblastoma. *Nat Med*. 2014;20:1035–42.
20. Iglesias-Bartolome R, Torres D, Marone R, et al. Inactivation of a Galpha(s)-PKA tumour suppressor pathway in skin stem cells initiates basal-cell carcinogenesis. *Nat Cell Biol*. 2015;17:793–803.
21. Zauber P, Marotta SP, Sabbath-Solitare M. GNAS gene mutation may be present only transiently during colorectal tumorigenesis. *Int J Mol Epidemiol Genet*. 2016;7:24–31.
22. Felsenstein M, Noe M, Masica DL, et al. IPMNs with co-occurring invasive cancers: neighbours but not always relatives. *Gut*. 2018;67:1652–62.
23. Omori Y, Ono Y, Tanino M, et al. Pathways of progression from intraductal papillary mucinous neoplasm to pancreatic ductal adenocarcinoma based on molecular features. *Gastroenterology*. 2019;156:647–61 e2.
24. Noe M, Niknafs N, Fischer CG, et al. Genomic characterization of malignant progression in neoplastic pancreatic cysts. *Nat Commun*. 2020;11:4085.
25. Kamiyama H, Kamiyama M, Hong SM, et al. In vivo and in vitro propagation of intraductal papillary mucinous neoplasms. *Lab Invest*. 2010;90:665–73.
26. Ran FA, Hsu PD, Wright J, et al. Genome engineering using the CRISPR-Cas9 system. *Nat Protoc*. 2013;8:2281–308.
27. Subramanian A, Tamayo P, Mootha VK, et al. Gene set enrichment analysis: a knowledge-based approach for interpreting genome-wide expression profiles. *Proc Natl Acad Sci U S A*. 2005;102:15545–50.
28. Schneider CA, Rasband WS, Eliceiri KW. NIH Image to ImageJ: 25 years of image analysis. *Nat Methods*. 2012;9:671–5.
29. Liberzon A, Birger C, Thorvaldsdottir H, et al. The molecular signatures database (MSigDB) hallmark gene set collection. *Cell Syst*. 2015;1:417–25.
30. De La OJ, Emerson LL, Goodman JL, et al. Notch and Kras reprogram pancreatic acinar cells to ductal intraepithelial neoplasia. *Proc Natl Acad Sci U S A*. 2008;105:18907–12.
31. Thomas MM, Zhang Y, Mathew E, et al. Epithelial Notch signaling is a limiting step for pancreatic carcinogenesis. *BMC Cancer*. 2014;14:862.
32. Komatsu H, Tanji E, Sakata N, et al. A GNAS mutation found in pancreatic intraductal papillary mucinous neoplasms induces drastic alterations of gene expression profiles with upregulation of mucin genes. *PLoS ONE*. 2014;9:e87875.
33. Zhang H, Kong Q, Wang J, et al. Complex roles of cAMP-PKA-CREB signaling in cancer. *Exp Hematol Oncol*. 2020;9:32.
34. Pattabiraman DR, Bierie B, Kober KI, et al. Activation of PKA leads to mesenchymal-to-epithelial transition and loss of tumor-initiating ability. *Science*. 2016;351:aad3680.
35. Pan Y, Wang C, Wang B. Phosphorylation of Gli2 by protein kinase A is required for Gli2 processing and degradation and the Sonic hedgehog-regulated mouse development. *Dev Biol*. 2009;326:177–89.
36. Djouder N, Tuerk RD, Suter M, et al. PKA phosphorylates and inactivates AMPKalpha to promote efficient lipolysis. *EMBO J*. 2010;29:469–81.
37. McGill MA, McGlade CJ. Mammalian numb proteins promote Notch1 receptor ubiquitination and degradation of the Notch1 intracellular domain. *J Biol Chem*. 2003;278:23196–203.
38. Lahiry M, Kumar S, Hari K, et al. AMPK-Fyn signaling promotes Notch1 stability to potentiate hypoxia-induced breast cancer stemness and drug resistance. *BioRxiv*. 2020. <https://doi.org/10.2139/ssrn.3586992>.
39. Greer RL, Staley BK, Liou A, et al. Numb regulates acinar cell dedifferentiation and survival during pancreatic damage and acinar-to-ductal metaplasia. *Gastroenterology*. 2013;145:1088–97.e8.
40. Inaguma S, Kasai K, Ikeda H. GLI1 facilitates the migration and invasion of pancreatic cancer cells through MUC5AC-mediated attenuation of E-cadherin. *Oncogene*. 2011;30:714–23.
41. Valque H, Gouyer V, Gottrand F, et al. MUC5B leads to aggressive behavior of breast cancer MCF7 cells. *PLoS ONE*. 2012;7:e46699.
42. Leir SH, Harris A. MUC6 mucin expression inhibits tumor cell invasion. *Exp Cell Res*. 2011;317:2408–19.
43. Yang KS, Ciprani D, O’Shea A, et al. Extracellular vesicle analysis allows for identification of invasive IPMN. *Gastroenterology*. 2021;160:1345–5811.
44. Huang Y, Nahar S, Nakagawa A, et al. Regulation of GLI underlies a role for BET bromodomains in pancreatic cancer growth and the tumor microenvironment. *Clin Cancer Res*. 2016;22:4259–70.
45. Wilson CH, McIntyre RE, Arends MJ, et al. The activating mutation R201C in GNAS promotes intestinal tumorigenesis in Apc(Min/+) mice through activation of Wnt and ERK1/2 MAPK pathways. *Oncogene*. 2010;29:4567–75.
46. Nomura R, Saito T, Mitomi H, et al. GNAS mutation as an alternative mechanism of activation of the Wnt/beta-catenin signaling pathway in gastric adenocarcinoma of the fundic gland type. *Hum Pathol*. 2014;45:2488–96.
47. O’Hayre M, Vazquez-Prado J, Kufareva I, et al. The emerging mutational landscape of G proteins and G-protein-coupled receptors in cancer. *Nat Rev Cancer*. 2013;13:412–24.
48. Coles GL, Cristea S, Webber JT, et al. Unbiased proteomic profiling uncovers a targetable GNAS/PKA/PP2A axis in small cell lung cancer stem cells. *Cancer Cell*. 2020;38:129–43.e7.
49. Zimmerman NP, Roy I, Hauser AD, et al. Cyclic AMP regulates the migration and invasion potential of human pancreatic cancer cells. *Mol Carcinog*. 2015;54:203–15.
50. Wehbe N, Slika H, Mesmar J, et al. The role of Epac in cancer progression. *Int J Mol Sci*. 2020;21:6489.
51. Almahariq M, Chao C, Mei FC, et al. Pharmacological inhibition and genetic knockdown of exchange protein directly activated by cAMP 1 reduce pancreatic cancer metastasis in vivo. *Mol Pharmacol*. 2015;87:142–9.
52. Avila JL, Kissil JL. Notch signaling in pancreatic cancer: oncogene or tumor suppressor? *Trends Mol Med*. 2013;19:320–7.

Publisher’s Note Springer Nature remains neutral with regard to jurisdictional claims in published maps and institutional affiliations.